Modelling the behaviour of a Hall current plasma accelerator

J Ashkenazy†, A Fruchtman‡, Y Raitses§|| and N J Fisch§

† Propulsion Physics Laboratory, Soreq NRC, Yavne 81800, Israel
‡ Center for Technological Education Holon, Holon 58102, Israel
§ Princeton Plasma Physics Laboratory, Princeton University, Princeton, NJ 08543, USA

Abstract. A simple model for the operation of the Hall current plasma accelerator, a crossed field discharge device that accelerates a flow of quasi-neutral plasma, is used to calculate the performance of an actual device at various configurations and operating conditions. The solutions demonstrate that the performance, characterized by the ionized fraction of the flow, the mass-averaged exit flow velocity and the total efficiency, improves as the flow rate or the accelerator length are increased at a given discharge voltage, trends that were also observed experimentally. Nevertheless, the calculated values for the longer lengths, especially the total efficiencies, are significantly higher than the measured ones, indicating the importance of an accurate solution of the electron energy equation and the need to include in the model plasma–wall interactions.

1. Introduction

The Hall current plasma accelerator is a crossed field discharge device that accelerates a high flux of quasi-neutral plasma. Typically this is done by axial electric and radial magnetic fields in an annular channel but other schemes are also feasible. The magnetic field serves to reduce the axial electron mobility while the electric field accelerates the ions in the axial direction. The working gas, entering the channel at the anode end, is ionized by impacts with those electrons which diffuse across the magnetic field. Although the research and development of Hall current plasma accelerators were pursued since the late 1950s [1–16], there is in recent years an increased interest in these devices, mainly as small rocket engines (electric thrusters) for space applications, where thrust is generated as a reaction to the momentum carried by the plasma jet emerging from the channel open end. Usually, such a device uses xenon as the working gas (propellant) and operates continuously at a discharge voltage of a few hundred volts and a current of a few amperes. Although the thrust is small (typically 0.01 N–1 N), the large jet velocity unattainable by chemical rocket engines ($10\,000$–$30\,000$ m s^{-1} against 2000–4800 m s^{-1}), results in a large saving in propellant mass. Operating with various working gases or gas mixtures, Hall current plasma accelerators could also be useful in industrial applications, when a high flux plasma is desired.

A Soreq built experimental accelerator is being used to study the physics of these devices and the dependence on design and operational parameters [17–20]. Of great interest is the coupling between the ionization and acceleration processes, thruster stability, plasma–wall interaction and the dynamic of the emerging jet. One purpose of the research is to obtain scaling relations which could be useful in the design of such devices to operate according to

|| Permanent address: Propulsion Physics Laboratory, Soreq NRC, Yavne 81800, Israel.

various requirements. So far, the accelerator behaviour was investigated in a broad range of operating conditions, i.e. discharge voltage, working gas flow rate and magnetic field strength, and under various modifications of channel geometry and wall material and magnetic profile, using electrical, magnetic and plasma diagnostics, as well as accurate thrust measurements. Extensive as these studies were, it would be useful to have a simple theoretical model, capturing the physics that governs the accelerator behaviour, which will allow us to perform fast parametric studies. The already obtained measured results would serve to test and refine the model.

As a first step towards this goal, we have recently started to develop a one-dimensional (1D) steady state model for Hall current plasma accelerators [21]. In the model, described later in section 2, the ions are treated as a cold fluid with the continuity equation having a source term representing the ion production process, which introduces also an effective drag term in the momentum equation. The electron dynamics are governed by the magnetic field, the electron pressure and diffusion across the magnetic field due to collisions. We note that the combination of the ion and electron equations results in a sonic transition singularity. At present, the electron temperature is assumed to be uniform along the channel and wall collisions are neglected. One of our goals in the present paper is to check the effect of these assumptions which much simplify the calculations, as also described in [21]. We look for steady-state solutions where the axial profile of the radial magnetic field, the channel geometry, the discharge voltage, the working gas flow rate, the neutral axial velocity and the electron temperature are specified. We assume also that the ion current at the anode is zero, corresponding to a monotonically decreasing potential from the anode to the cathode. We then solve for the axial dependence of the electric potential, the plasma and neutral densities and the electron and ion currents. The discharge current is determined by the requirement of regularity and smoothness of the solutions through the sonic transition point.

The model was used to calculate the accelerator behaviour in a broad range of operating conditions. In section 3, we summarize the results by presenting calculated values of three parameters characterizing the accelerator performance: the ionized fraction of the flow rate, the mass-averaged exit velocity (specific impulse) and the overall efficiency. The results have demonstrated that all three parameters improve as the flow rate or the channel length are increased at a given discharge voltage, trends that were also observed experimentally. Nevertheless, the calculated values for the longer lengths, especially the total efficiencies, are significantly higher than the measured ones, indicating the importance of an accurate solution of the electron energy equation and the need to include in the model plasma–wall interactions.

2. The model

A schematic drawing of an annular Hall current plasma accelerator is shown in figure 1. It consists of a dielectric channel, an anode, a magnetic circuit (details not shown) which generates a radial magnetic field in the channel and an external hollow cathode. In the proper operating regime of such a device the electron Hall parameter is larger than unity and the electron Larmor radius is small compared to a typical channel dimension, i.e. the electrons are magnetized. On the other hand, the Larmor radius of the much heavier ions is larger than the channel dimension and so they are not practically affected by the magnetic field. Under the influence of the axial electric and radial magnetic fields the electrons drift in the azimuthal direction (azimuthal Hall current). Due to collisions, electrons diffuse across the magnetic field towards the anode (axial electron current) and ionize by impacts the working gas atoms emerging from the anode. The axial dependence of the axial electron mobility, which is controlled by the magnetic field profile, determine the electric potential drop. In a preferred configuration, the magnetic field
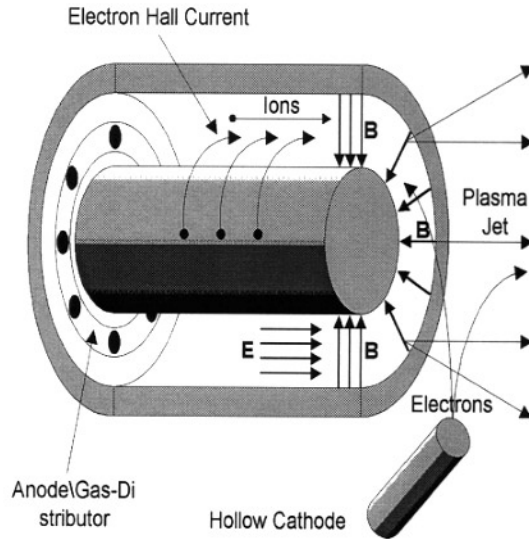
Figure 1. A schematic drawing of the annular Hall current plasma accelerator.

is minimal near the anode and increases towards the channel exit [6, 19]. As a result, most of the potential drop is concentrated near the exit. Consequently, it is expected that effective acceleration will start downstream the region where a substantial fraction of the flow is ionized and will take place along a short distance near the exit, thus maximizing the utilization of the electric potential for acceleration and minimizing ion losses due to wall collisions.

Contrary to [21], where we were mainly interested in general scaling laws, we present here the model equations in a dimensional form. Provided that the operating conditions described earlier prevail, the 1D steady-state electron dynamics equation is given by

$$v_{ez} = \mu \left(-\frac{d\Phi}{dz} + \frac{k}{en_e} \frac{d(T_e n_e)}{dz} \right) \tag{1}$$

where Φ is the electric potential, e, n_e, T_e and v_{ez} are, respectively, the electron charge, density, temperature and axial velocity, k is the Boltzmann constant and $\mu = ev/m\omega_c^2$ is the electron mobility across the magnetic field. m is the electron mass while v and ω_c are respectively the electron collision and cyclotron frequencies. The ion continuity equation includes a source term representing ion production

$$\frac{d(n_i v_i)}{dz} = n_e n_0 \beta \tag{2}$$

where n_i and v_i are, respectively, the ion density and velocity, n_0 is the neutral density, and β is the average of σv_e, where σ is the ionization cross section. Quasi-neutrality is assumed. The cold fluid ion momentum equation is given by

$$M v_i \frac{dv_i}{dz} + e \frac{d\Phi}{dz} = -M n_0 v_i \beta. \tag{3}$$

Note the effective drag term due to ion production on the right-hand side.

In the present form of the model, T_e is assumed to be constant, thus much simplifying by avoiding the need for an energy equation. T_e is specified based on past measurements on similar devices and theoretical considerations [5, 7, 22], which indicate that the electron

temperature is proportional to the discharge voltage, $kT_e \approx 0.1\Phi_d$. As in actual experiments, the accelerator configuration is determined by the channel length, L, and cross sectional area, A, and by the magnetic field profile, while a specific working point is externally determined by the applied discharge voltage, Φ_d, the working gas mass flow rate, $\dot{m}$, and by the magnetic field strength, which in the experiments is controlled by varying the current in the magnetic circuit coils. In the solution, we use also the conservation of the mass flux, $\dot{m} = (n_0 v_a + n_i v_i)MA$, and the total discharge current, $I_d = en_e(v_i + v_{ez})A$, where v_a is the neutral flow velocity, assumed constant. We then have to solve equations (1)–(3) for Φ, n_e, v_i and v_{ez}. The boundary conditions are $\Phi(0) = \Phi_d$, $\Phi(L) = 0$, and $I_i(0) = 0$, where I_i is the ion current. The last condition assumes a monotonically decreasing potential from the anode to the cathode and excludes the possibility of backward ion flow.

Equations (1)–(3) can be combined to give

$$(2v_i^2 - C_s^2)\frac{dn_e}{dz} = 4v_i n_e n_0 \beta - \frac{2en_e v_{ez}}{M\mu}. \tag{4}$$

As can be seen, equation (4) is singular at the sonic transition point, where the ion velocity is equal to the ion acoustic velocity, $C_s = \sqrt{2T_e/M}$. In solving equations (1)–(3), we choose to look for solutions that are regular at the sonic transition point. This is done by requiring that the right-hand side of equation (4) will vanish at the sonic transition point. This requirement determines the value of I_d. The location of the sonic transition is found by a shooting method, which assures also that the specified boundary conditions are satisfied. While there are no firm theorems for either the uniqueness or the existence of solutions, we do succeed, in practice, in finding regular solutions to equations (1)–(3) with the specified boundary conditions.

In the experiments, when the magnetic field is increased for given discharge voltage and mass flow rate values, the discharge current tends to drop, indicating a drop in the axial electron current due to the reduced axial electron mobility. If, however, the magnetic field strength is raised beyond a certain point, the discharge current typically increases again, a behaviour which is associated with the appearance of current and voltage oscillations, which can become strong enough to prevent stable operation of the device. Such a dependence of the discharge current on the magnetic field strength is typical for Hall accelerators [4, 7, 17, 19]. The minimum discharge current point is usually the point of maximum efficiency (see later), and consequently the preferred working point. In a manner similar to experiment, we look first for a solution to our steady-state model equations for given Φ_d and $\dot{m}$ values and a relatively large value of the amplitude of the axial electron mobility. Then, this mobility is reduced and the process is repeated, until we reach a point beyond which a (steady-state) solution is not found.

3. Modelling the performance of an actual device

In the present work we were mainly interested in the performance of the Hall current plasma accelerator as a thruster. Parameters characterizing that performance can be obtained from the solutions to equations (1)–(3) at specific operating points. One such parameter is the ionized fraction of the mass flow

$$\eta_p = \frac{MAn_i v_i}{\dot{m}} \tag{5}$$

where n_i and v_i are taken here at the channel exit. Since effectively the velocity of neutrals is negligible compared to that of ions at the exit, η_p is referred to as the propellant (working gas) utilization factor. Another parameter of prime importance is the specific impulse, i.e. the mass averaged flow velocity at the exit, which strongly affects the required propellant mass onboard

spacecraft, $Isp \equiv T/\dot{m}g$, where T is the thrust. We have used here the common definition of Isp, where it is divided by the acceleration of gravity at sea level and expressed in seconds. Again, neglecting the neutral velocity we can write

$$Isp = \frac{MAn_i v_i^2}{\dot{m}g} = \frac{\eta_p v_i}{g}. \tag{6}$$

Since spacecraft are usually power limited systems, the total efficiency, defined as the ratio of the kinetic power of the emerging flux to the input electric power, is also of importance

$$\eta_T = \frac{(1/2)\dot{m}(gIsp)^2}{I_d\Phi_d} = \eta_p \frac{I_i}{I_d} \frac{(1/2)Mv_i^2}{e\Phi_d}. \tag{7}$$

The calculation results we present later refer to a Soreq built Hall current plasma accelerator whose behaviour was characterized at similar operating conditions. The accelerator, the experimental set up and the measurements are described in detail in [17–19]. This device has a channel cross sectional area, A, of 25 cm^2. The effective length of the channel can be varied by changing the position of the anode in the channel. Here, operation at three lengths, $L = 20, 30, 40$ mm with a xenon propellant is investigated with the model calculations. The profile of the magnetic field along the median is shown in figure 2. The channel exit is at $z = 40$ mm. Hence, the anode was located at $z = 0$ mm for the $L = 40$ mm case, at $z = 10$ mm for the $L = 30$ mm case and at $z = 20$ mm for the $L = 20$ mm case. The measured profile was best-fitted to a seven-term rational function which was used as an analytical expression in the model calculations.
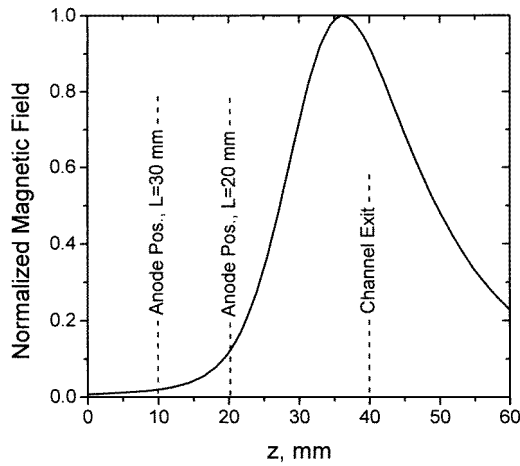
Figure 2. The magnetic profile along the median of the accelerator channel. The same profile was used in the 1D model calculations. For the channel length cases, $L = 20, 30, 40$ mm, the anode was located at $z = 0, 10, 20$ mm respectively.

In the experiments, the thrust, measured with a pendulum type thrust stand [17–19] and the ion current, obtained by integration over the angular distribution of the ion flux measured with a planar Langmuir probe [17–19], together with the measured input power and mass flow rate, were used to deduce the experimental values of η_p, Isp and η_T.

As mentioned earlier, the energy equation is not included in the present version of the model. Nevertheless, since the cross section for ionization of xenon atoms by impact electrons changes rapidly in the range of 10–30 eV, we took care for the slow down of electrons as

they diffuse towards the anode by introducing for β a phenomenological dependence of the form

$$\beta = \beta_0 \frac{1 - e^{-\alpha \dot{m} L}}{\alpha \dot{m} L} \tag{8}$$

where $\beta_0 = 1.26 \times 10^{-7}$ cm^3 s^{-1} at 30 eV [23] and α is a phenomenological 'slow down' parameter obtained by trying to best-fit the calculation results to the measured values of propellant utilization (the parameter that determines the efficiency of the ionization) for the 20 mm case. Such a functional dependence on $\dot{m}$ and L is introduced assuming that the slow down of electrons increases with the number of collisions they encounter, which depends on the distance they have to travel and as well on the density of particles.

The results of calculation are summarized in figure 3 showing the propellant utilization, total efficiency and specific impulse against the mass flow rate for $L = 20, 30, 40$ mm and $\Phi_d = 300$ V. As can be seen, the performance in all three parameters improves as L or $\dot{m}$ are increased. This behaviour is interpreted as being mainly due to the improved ionization probability as the distance the neutral atoms have to travel or the particle density in the channel become larger, resulting in a larger propellant utilization. Such trends were, in general, observed also experimentally [18, 19]. The measured performance values at similar operating conditions are shown in figure 4. As can be seen, however, at the longer channel length cases, the calculated performance, especially the total efficiency, reaches values which are significantly higher than the measured ones. Moreover, the measured performance for $L = 40$ mm improves with $\dot{m}$ at a lower rate than for the $L = 30$ case, and even becomes smaller for $\dot{m} \geqslant 1.8$ mg s^{-1}, a behaviour which is not demonstrated by the calculations. These discrepancies can be interpreted in terms of length dependent loss mechanism(s) which are not included in the model. One such mechanism is ion recombination at the channel walls acting as a third large body. As for the larger discrepancies in the total efficiency, η_T depends also on the current ratio I_i/I_d (see equation (7)) which in the calculations reaches values of 0.95 for $L = 30$ mm and 0.98 for $L = 40$ mm at large mass flow rates, while in the experiments maximal values of only 0.6–0.7, depending on channel material, were obtained [19]. In part,
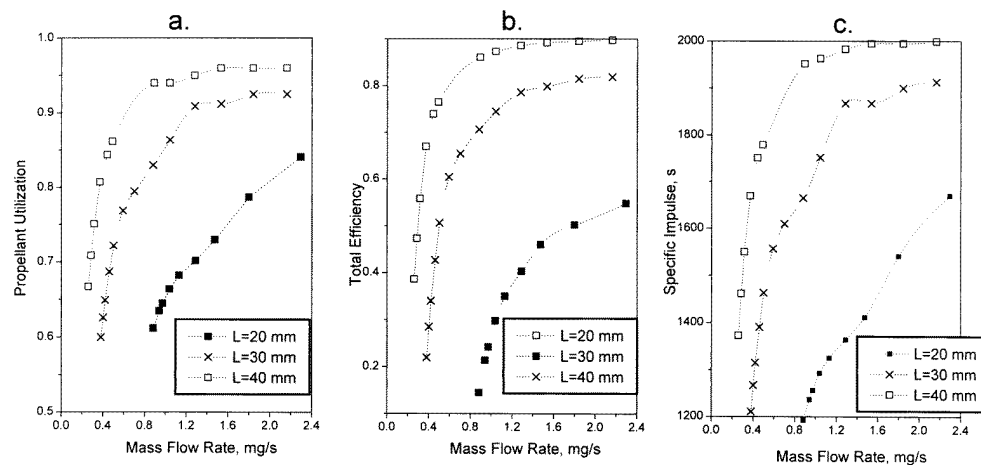
Figure 3. Calculated performance against mass flow rate for a discharge voltage of 300 V and three channel lengths: 20, 30, 40 mm. (a) Propellant utilization; (b) total efficiency; and (c) specific impulse.
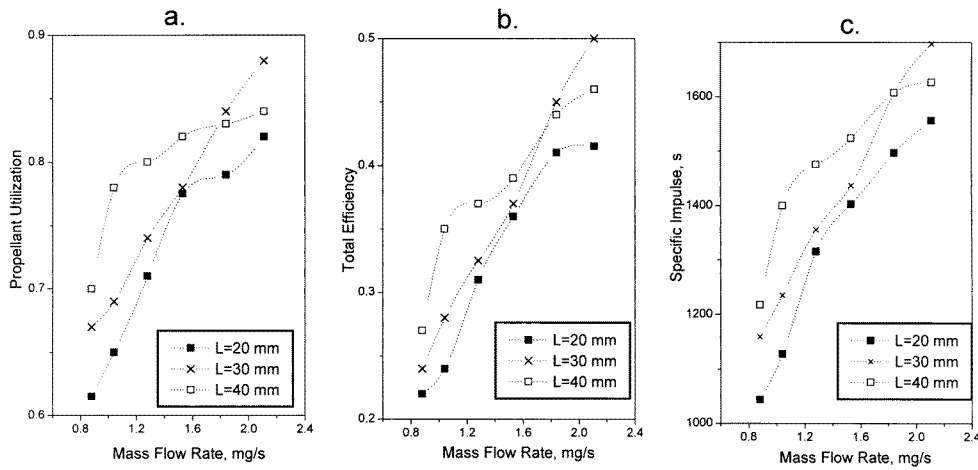
Figure 4. Measured performance against mass flow rate for a discharge voltage of 300 V and three channel lengths: 20, 30, 40 mm. (a) Propellant utilization; (b) total efficiency; and (c) specific impulse.

this discrepancy serves as another indication for the existence of a parasitic electron current which is a result of wall interaction [9, 19] of some sort, the nature of which is currently being investigated by us. It could also be a result of not taking into account the slow down of electrons in a consistent way, which in cases when the mean free path of electrons is much smaller than the channel length (large mass flow rate) results in a too small electron current effectively ionizing the mass flow. This problem is expected to be solved by the inclusion of the energy equation in the model.

4. Summary

A 1D steady-state model for the operation of the Hall current plasma accelerator was described. The unmagnetized ions are treated as a cold fluid, while the electron dynamics is governed by the magnetic field, electron pressure and by diffusion across the magnetic field. The ionization process is incorporated into the ion continuity and momentum equations. In the present version of the model, plasma–wall interaction is not included and the electron temperature is assumed to be constant. In the process of solution, the sonic transition singularity is removed and the strength of the magnetic field is optimized in a manner analogous to the way it is done in the experiment. The model was used to calculate the performance of an actual device for three channel length configurations, $L = 20, 30, 40$ mm, at a discharge voltage of 300 V and a range of xenon mass flow rate values. The results of these calculations have demonstrated that the propellant utilization (the ionized fraction of the flow), the specific impulse (the mass averaged exit flow velocity) and the total efficiency improve as the flow rate or the channel length are increased, a trend that was already demonstrated experimentally. However, the values predicted by the calculations, especially those of the total efficiency, become significantly higher than the measured ones for the longer channel cases. This seems to be a result of the sensitivity of the cross sections to the electron temperature in the relevant range, and the existence of length dependent loss mechanism(s), most probably associated with wall interactions. The inclusion of accurate solutions of the electron energy equation and treatment of plasma–wall interaction are planned for the next stage of model development.

References

[1] Morozov P M 1958 *Physics and Problems of Controlled Fusion* vol 4 (Moscow: USSR Academy of Science) pp 235–57 (in Russian)

[2] Janes G S, Dotson J and Wilson T 1962 *Proc. 3rd Symp. on Advanced Propulsion Concepts* vol 1 (London: Gordon and Breach) pp 153–73

[3] Etherington R J and Haines M G 1965 *Phys. Rev. Lett.* **14** 15

[4] Morozov A I, Esinchuck Yu, Tilinin G, Trofimov A, Sharov Yu and Shchepkin G 1972 *Sov. Phys.–Tech. Phys.* **17** 38

[5] Bishaev A M and Kim V 1978 *Sov. Phys.–Tech. Phys.* **23** 1055

[6] Gavryushin V M and Kim V 1981 *Sov. Phys.–Tech. Phys.* **26** 505

[7] Bugrova A I and Kim V 1984 *Plasma Accelerators and Ion Injectors* (Moscow: Nauka) pp 107–29 (in Russian)

[8] Kaufman H R 1985 *AIAA* **23** 78

[9] Bugrova A I, Morozov A I and Kharchevnikov V K 1990 *Sov. J. Plasma Phys.* **16** 849

[10] Bugrova A I, Maslenikov N A and Morozov A I 1991 *Sov. Phys.–Tech. Phys.* **36** 612

[11] Lentz C A and Martinez-Sanchez M 1993 *29th Joint Propulsion Conf. (Monterey, CA)* AIAA paper 93-2491

[12] Choueiri E Y 1994 *30th Joint Propulsion Conf. (Indianapolis, IN)* AIAA paper 94-3013

[13] Komurasaki K, Mikami K and Kusamoto D 1996 *32nd Joint Propulsion Conf. (Lake Buena Vista, FL)* AIAA paper 96-3194

[14] Hirakawa M and Arakawa Y 1996 *32nd Joint Propulsion Conf. (Lake Buena Vista, FL)* AIAA paper 96-3195

[15] Oh D and Hastings D 1996 *32nd Joint Propulsion Conf. (Lake Buena Vista, FL)* AIAA paper 96-3196

[16] Khayms V and Martinez-Sanchez M 1996 *32nd Joint Propulsion Conf. (Lake Buena Vista, FL)* AIAA paper 96-3291

[17] Ashkenazy J, Raitses Y and Appelbaum G 1995 *31st Joint Propulsion Conf. (San Diego, CA)* AIAA paper 95-2673

[18] Raitses Y, Ashkenazy J and Guelman M 1998 *AIAA J. Prop. Power* **14** 247

[19] Ashkenazy J, Raitses Y and Appelbaum G 1998 *Phys. Plasmas* **5** 2055

[20] Raitses Y, Ashkenazy J and Appelbaum G 1998 *34th Joint Propulsion Conf. (Cleveland, OH)* AIAA paper 98-3640

[21] Fruchtman A, Fisch N J, Ashkenazy J and Raitses Y 1997 *25th Int. Electric Propulsion Conf. (Cleveland, OH)* IEPC paper 97-022

[22] Ashkenazy J, Raitses Y and Appelbaum G 1997 *Proc. 2nd Eur. Spacecraft Propulsion Conf.* (Nordwijk: ESA Publication Division) pp 455–60

[23] Perkins S T, Cullen D E and Seltzer S M 1991 *Tables and Graphs of Electron-Interaction Cross Sections from 10 eV to 100 GeV. Derived from the LLNL Evaluated Electron Data Library (EEDL), Z = 1–100* vol 31, UCRL-50400